Chinese Journal of Chemical Engineering 28 (2020) 593–597

Contents lists available at ScienceDirect

Chinese Journal of Chemical Engineering

journal homepage: www.elsevier.com/locate/CJChE

Article

Reversed ethane/ethylene adsorption in a metal–organic framework *via* introduction of oxygen

Ling Yang [1], Wei Zhou [2], Hao Li [3], Ali Alsalme [4], Litao Jia [5], Jiangfeng Yang [1], Jinping Li [1], Libo Li [1,5,6,7,*], Banglin Chen [3,*]

[1] College of Chemistry and Chemical Engineering, Shanxi Key Laboratory of Gas Energy Efficient and Clean Utilization, Taiyuan University of Technology, Taiyuan 030024, PR China
[2] NIST Center for Neutron Research, National Institute of Standards and Technology, Gaithersburg, MD 20899-6102, United States
[3] Department of Chemistry, University of Texas at San Antonio, One UTSA Circle, San Antonio, TX 78249-0698, United States
[4] Chemistry Department, College of Science, King Saud University, P O Box 2455, Riyadh 11451, Saudi Arabia
[5] State Key Laboratory of Coal Conversion, Institute of Coal Chemistry, Chinese Academy of Sciences, Taiyuan 030024, China
[6] Key Laboratory of Coal Science and Technology, Taiyuan University of Technology, Taiyuan 030024, China
[7] Shanxi Key Laboratory of Gas Energy Efficient and Clean Utilization, Taiyuan 030024,China

ARTICLE INFO

Article history:
Received 1 August 2019
Received in revised form 3 September 2019
Accepted 5 September 2019
Available online 15 October 2019

Keywords:
Metal–organic frameworks
Adsorptive separation
Open metal sites
Reversed ethane/ethylene adsorption
Density-functional theory calculation
Breakthrough curves

ABSTRACT

Separation of ethane from ethylene is a very important but challenging process in the petrochemical industry. Finding an alternative method would reduce the energy needed to make 170 million tons of ethylene manufactured worldwide each year. Adsorptive separation using C_2H_6-selective porous materials to directly produce high-purity C_2H_4 is more energy-efficient. We herein report the "reversed C_2H_6/C_2H_4 adsorption" in a metal–organic framework Cr-BTC *via* the introduction of oxygen on its open metal sites. The oxidized Cr-BTC(O_2) can bind C_2H_6 over C_2H_4 through the active Cr-superoxo sites, which was elucidated by the gas sorption isotherms and density functional theory calculations. This material thus exhibits a good performance for the separation of 50/50 C_2H_6/C_2H_4 mixtures to produce 99.99% pure C_2H_4 in a single separation operation.

1. Introduction

Ethylene (C_2H_4) is a crucial starting chemical for the manufacture of many high-value organic products. In production plants, C_2H_4 is usually produced by thermal decomposition of ethane (C_2H_6) and steam cracking of naphtha. C_2H_6 will inevitably arise in these processes. Before plastic manufacturing process, separating C_2H_6 to produce polymer-grade (≥99.95% pure) C_2H_4 is very challenging, due to their similar molecular sizes and volatilities [1,2]. The current well-established method of producing this chemical is using a cryogenic high-pressure distillation process, which takes lots of energy in chemical industry. So developing an energy-efficient C_2H_6/C_2H_4 separation process is highly desired and is among the most important industrial separation processes in future [3].

Nonthermal adsorbent-based separation seems to be a promising alternative method in recent years, with low energy requirements and operating costs [4–6]. However, conventional porous materials such as zeolites and carbon-based materials are not satisfactory in this separation process due to poor adsorption selectivity and low capacity. As novel porous materials, metal–organic frameworks (MOFs) have attracted immense attention from both academia and industry in recent decades due to their excellent gas separation performance [7–19]. Unlike traditional porous materials, the pore surface and gas diffusion channels of MOFs could be easily functionalized and designed [20–30], which enables them to show promise for a wide variety of gas separation areas, including the important C_2H_6/C_2H_4 separation.

According to different binding affinities for C_2H_6 or C_2H_4, MOFs can be cataloged into C_2H_4-selective MOFs and C_2H_6-selective one in C_2H_6/C_2H_4 separation. Generally, C_2H_4-selective MOFs have polar binding centers like open metal sites (OMSs) [31] or narrow pore channels (0.3–0.4 nm) [32] that can selectively capture C_2H_4 from C_2H_6/C_2H_4 mixtures. But these adsorbents usually require three or four additional separation cycles to yield high-purity C_2H_4 product [1], which significantly increases the energy consumption of this method. The latter C_2H_6-selective MOFs is proposed to be much more efficient. C_2H_4 is afforded directly through a single adsorption step, which simplifies the process and results in high separation productivity [33,34]. However, construction of C_2H_6-selective MOFs is more challenging in view of the non-polarity and larger molecular size of C_2H_6 (C_2H_4: 0.48 × 0.42 × 0.33 nm^3, C_2H_6: 0.48 × 0.41 ×

* Corresponding authors at: College of Chemistry and Chemical Engineering, Taiyuan University of Technology, Taiyuan 030024, China.
E-mail addresses: lilibo908@hotmail.com (L. Li), banglin.chen@utsa.edu (B. Chen).

https://doi.org/10.1016/j.cjche.2019.09.005
1004-9541/

0.38 nm^3) [32]. Only a few examples have been identified so far, and they suffer from poor selectivities owing to lack of suitable strong binding sites for C_2H_6 [35–37]. In 2018, we reported a functionalized MOF [$Fe_2(O_2)$(dobdc)] with Fe–peroxo sites, which can induce stronger interactions with C_2H_6 than with C_2H_4 [38]. This strategy might provide us a tunable platform that can modify OMSs to realize ideal porous materials for C_2H_6/C_2H_4 separation. We thus synthesized Cr-BTC(O_2) [Cr_3(1,3,5-benzenetricarboxylate)$_2(O_2)_3$], developed by Murray *et al.* [39], studied its adsorption mechanisms for binding C_2H_6, and investigated the C_2H_6/C_2H_4 separation performance. In Cr-BTC(O_2), the O_2 was believed to be a superoxo $(O_2)^-$, not a peroxo $(O_2)^{2-}$. We suspected that it may exhibit similar effect toward gas binding. Indeed, with the modified superoxo group, this MOF can preferentially bind C_2H_6 over C_2H_4, leading to the unusual reversed C_2H_6/C_2H_4 adsorption. This material thus can capture C_2H_6 from C_2H_6/C_2H_4 mixture to yield polymer-grade C_2H_4 under ambient conditions, as demonstrated by experimental breakthrough results.

2. Experimental

2.1. Synthesis of materials

2.1.1. Cr-BTC [$Cr_3(BTC)_2$]

The synthetic method described by Murray *et al.* [39] was improved as follows: anhydrous $Cr(CO)_6$ (1.09 g, 5 mmol), trimesic acid (H_3BTC, 0.623 g, 3 mmol), and anhydrous DMF (50 ml) were added to a 100 ml three-neck flask in glove box filled with 99.999% N_2. The reaction mixture was heated to 393 K and stirred for three days to form purple precipitate. Methanol exchange was repeated six times during 2 days, and the solid was collected by filtration and dry in vacuum to yield $Cr_3(BTC)_2$ solvent as an orange powder. $Cr_3(BTC)_2$ solvent sample was fully activated by heating under dynamic vacuum ($<10^{-2}$ Pa) at 433 K for 24 h and then cooled down to room temperature to yield $Cr_3(BTC)_2$ as light green powder. $Cr_3(BTC)_2$ is air-sensitive, and needs to be handled and stored in a dry box under N_2 atmosphere.

2.1.2. Cr-BTC(O_2) [$Cr_3(BTC)_2(O_2)_3$]

$Cr_3(BTC)_2$ was oxidized under carefully controlled conditions: about 1 g $Cr_3(BTC)_2$ sample was transferred into a 500 ml flask in a dry glove box, then sealed and evacuated to 10^{-2} Pa. Pure O_2 (>99.999%) was slowly dosed to the bare $Cr_3(BTC)_2$ sample to 10^3 Pa at a rate of 50 Pa·min^{-1} under 298 K and kept it for 30 min. The O_2 pressure was brought up to 10^5 Pa and was maintained constant over 1 h to reach equilibrium. At last, the sample was evacuated to remove the free O_2 gas molecules and yield the deep green $Cr_3(BTC)_2(O_2)_3$. $Cr_2(BTC)_3(O_2)_3$ is air-sensitive, the water molecule in the air will cause its gradual destruction, so the sample needs to be handled in a dry box under N_2 atmosphere.

All chemical reagents and solvents were commercially available, and used without further purification.

2.2. Characterizations

The gas sorption isotherms were collected on an Intelligent Gravimetric Analyzer (IGA 001, Hiden, UK). The purities of the N_2, C_2H_4 and C_2H_6 are higher than 99.999%. To maintain the experimental temperatures, ice-water bath (273 K) and water bath (298 K) were used. The breakthrough curves were measured on a homemade apparatus; the details were provided in supporting information.

2.3. Density-functional theory calculation

Density-functional theory (DFT) calculations were performed to gain better understanding of the superoxo groups in the adsorption of C_2H_6 and C_2H_4. Due to the orientational disorder of the superoxo groups on the Cr metal sites, direct calculation based on the MOF crystal structure is not straightforward. In this work, we adopted a simplified cluster model to evaluate the gas binding. Each cluster consists of two Cr^{2+} ions and four H_2BTC^- groups, forming a charge-neutral Cr_2 paddlewheel. The cluster was put in a 2.5 nm × 2.5 nm × 25 nm supercell. For this system, a cutoff energy of 544 eV and a 2 × 2 × 2 *k*-point mesh (generated using the Monkhosrt-Pack scheme) were found to be enough for total energy to converge within 0.01 meV per atom. The cluster models (without and with superoxo sites) were first fully optimized with respect to atomic coordinates. The ground state of the Cr_2 dimer was found to be antiferromagnetic. For C_2H_6 or C_2H_4 adsorption, various possible binding configurations were considered and fully relaxed. The lowest-energy structures were identified as the optimal binding structures.

3. Results and Discussion

3.1. Structure analysis

Cr-BTC has a three-dimensional framework structure depicted in Fig. 1a, where Cr_2 paddlewheel complexes are linked *via* triangular BTC^{3-} to form an isostructural structure of Cu-BTC. The as-synthesized Cr-BTC sample was exchanged with methanol for six times, and heated at 433 K under vacuum over 48 h to fully expose the Cr(II) OMSs. Next, O_2 molecule was induced to bind Cr(II) OMSs under carefully controlled conditions to form the Cr-superoxo sites in Cr-BTC(O_2) (Fig. 1b and c). Cr-BTC(O_2) maintains the framework structure of Cr-BTC, with a Brunauer–Emmett–Teller surface area of 1135 $m^2 \cdot g^{-1}$ (Fig. S1a). Bulk purity of Cr-BTC(O_2) sample was confirmed by powder X-ray diffraction (PXRD) patterns, infrared spectroscopy analysis, and the measured surface area (Fig. S1).

3.2. Gas adsorption and separation

The C_2H_6 and C_2H_4 sorption isotherms of Cr-BTC and Cr-BTC(O_2) were collected at 273 and 298 K (Figs. 2 and S2). As shown in Fig. 2a and b, the C_2H_6 and C_2H_4 adsorption isotherms of Cr-BTC and Cr-BTC (O_2) show type I character with a smooth increase with pressure. At 10^5 Pa and 298 K, C_2H_4 and C_2H_6 adsorption capacities of Cr-BTC are 6.03 mmol·g^{-1} (135 $cm^3 \cdot g^{-1}$) and 5.27 mmol·g^{-1} (118 $cm^3 \cdot g^{-1}$), respectively. While, after O_2 molecule bonded, the selectivity of two gases is totally reversed. The gas uptakes of C_2H_6 and C_2H_4 on Cr-BTC(O_2) reach 3.30 mmol·g^{-1} (74 $cm^3 \cdot g^{-1}$) and 2.89 mmol·g^{-1} (65 $cm^3 \cdot g^{-1}$), respectively, at the same conditions. The corresponding isosteric heat (Q_{st}) of C_2H_6 adsorption on Cr-BTC(O_2) was calculated to be 37.2 kJ·mol^{-1} at zero coverage (Figs. 2d and S3), which is apparently higher than that of C_2H_4 (23.5 kJ·mol^{-1}). Furthermore, C_2H_6/C_2H_4 (50/50) selectivity of Cr-BTC(O_2) calculated by ideal adsorbed solution theory (IAST) is over 3 at the low pressure region, which decreases gradually as the pressure increases (Figs. 2e and S4). This is mainly due to the strong interactions between C_2H_6 molecules and Cr-superoxo sites at low pressure. According to these results, we further demonstrated the separation performance of Cr-BTC(O_2) for C_2H_6/C_2H_4 (50/50) mixtures under dynamic conditions. Breakthrough experiments were performed in a packed column containing ~1 g of Cr-BTC(O_2) samples at room temperature (298 K). As shown in Fig. 2c, the breakthrough data clearly demonstrate that Cr-BTC(O_2) can effectively separate C_2H_6/C_2H_4 mixtures: the C_2H_4 gas passed through the adsorption bed first, while C_2H_6 was retained in the packed column. The concentration of C_2H_6 in the outlet effluent was below 0.1%, thus producing C_2H_4 with a purity of >99.99%. To ensure the regenerability of Cr-BTC(O_2), C_2H_6/C_2H_4 (50/50) separation cycling experiments were performed at the same conditions (Fig. 2f). The experimental cycling results indicate that there was no noticeable loss of C_2H_6/C_2H_4 separation capacity in continuous 4 cycles.

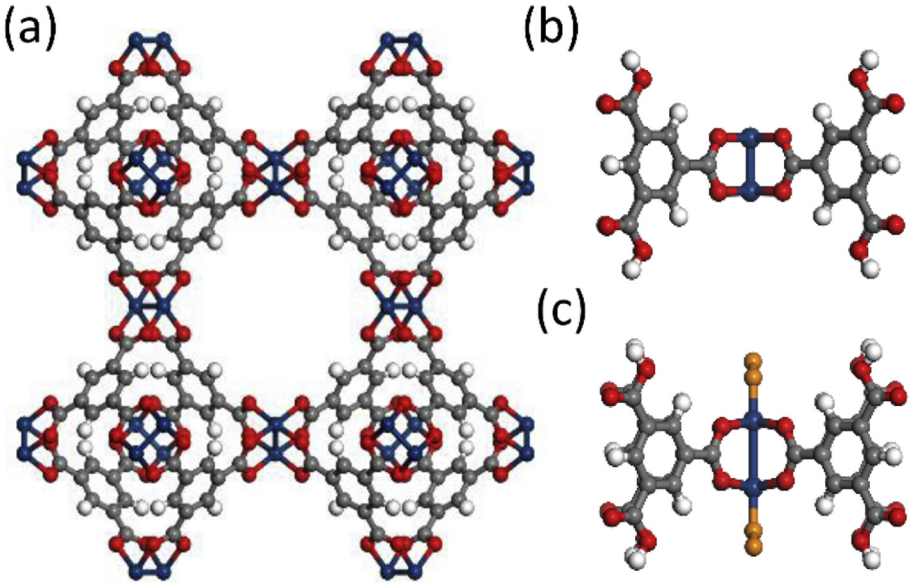

Fig. 1. (a) Illustration of the structure of Cr-BTC, and the cluster models of Cr_2BTC_4 (b) and $Cr_2BTC_4(O_2)_2$ (c) used in the calculations (Cr, navy; C, gray; O, red; O_2^-, orange, H, white) [39].

3.3. Density-functional theory calculation

To understand the special role of the superoxo groups in the adsorption of C_2H_6 and C_2H_4, we performed DFT calculations. Due to the orientational disorder of the superoxo groups on the Cr metal sites, direct calculation based on the MOF crystal structure is not straightforward. Therefore, we adopted a simplified cluster model to evaluate the gas binding. Our cluster model consists of two Cr^{2+} ions and four H_2BTC^- groups, forming a charge-neutral Cr_2 paddlewheel. We first calculated the C_2H_4 and C_2H_6 binding on the open Cr sites, and the optimized gas binding configurations are shown in Fig. 3(a, c).

As expected, C_2H_4 binds strongly to the open Cr site through the C=C bond in a side-on mode, while C_2H_6 binds to the open Cr site relatively weakly through one —CH_3 in an end-on configuration. The corresponding calculated static binding energies of the two molecules are 34.2 and 22.4 kJ·mol^{-1}, respectively. Next, O_2 molecules were introduced to the Cr sites to form a cluster model for Cr-BTC(O_2). Two different initial O_2 binding configurations (end-on and side-on) were considered. In both cases, the O_2 got relaxed to the same end-on binding configuration, suggesting that the end-on orientation of O_2 corresponds to the lowest energy configuration. The O—O bond length in the fully optimized structure is 0.128 nm, a typical value for superoxo species and slightly larger than that of molecular O_2 (0.121 nm). Inspection of the charge density distribution also shows that there is notable amount of charge transfer from Cr^{2+} to O_2, turning Cr^{2+} to nearly Cr^{3+}, and O_2 to $(O_2)^-$. These findings are consistent with the previously reported experimental results [39]. Subsequently, we calculated the gas binding on the structure where both Cr sites are pre-occupied by superoxo groups.

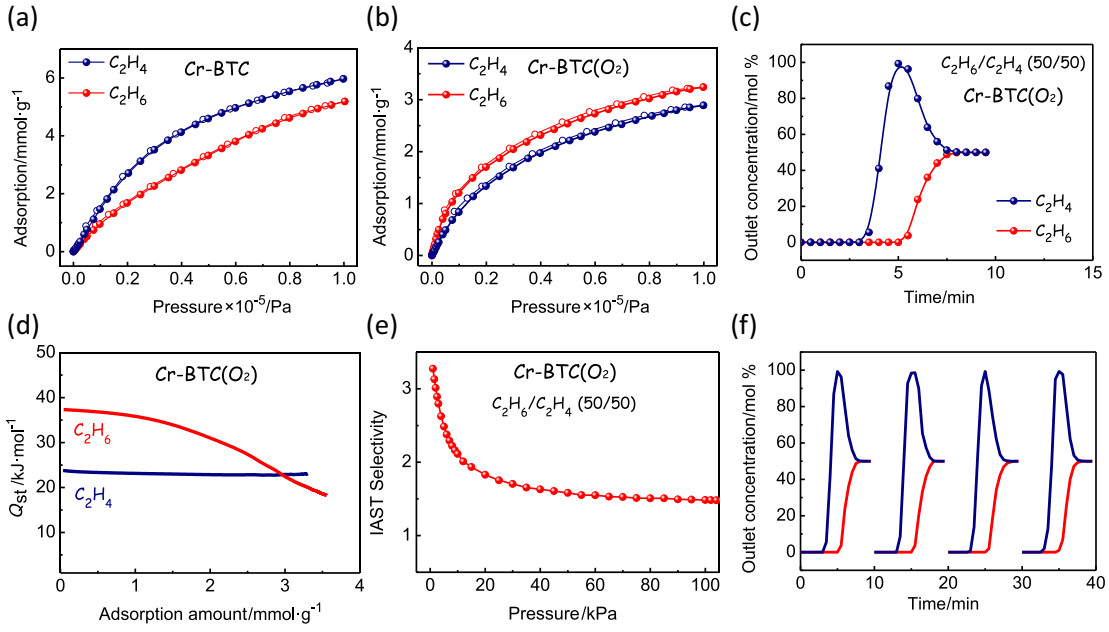

Fig. 2. (a, b) Experimental C_2H_6 and C_2H_4 sorption isotherms of Cr-BTC and Cr-BTC(O_2) at 298 K. (c) Breakthrough curves of 50/50 (v/v) C_2H_6/C_2H_4 mixture on Cr-BTC(O_2) at 298 K. (d) Isosteric heat of C_2H_6 and C_2H_4 adsorption on Cr-BTC(O_2). (e) Predicted mixture adsorption selectivity of Cr-BTC(O_2) predicted by IAST method at 298 K. (f) 50/50 C_2H_6/C_2H_4 separation cycles lasting for 40 min. Each separation process was carried out at 298 K and 1.01 bar, while regeneration was performed using vacuum at 298 K for 2 min.

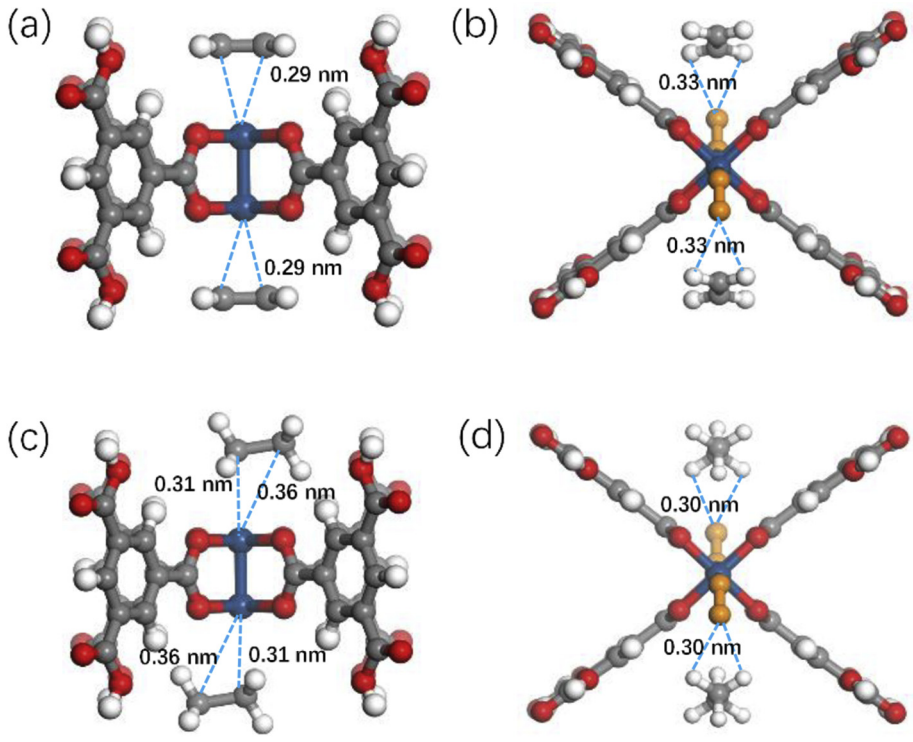

Fig. 3. The preferential C_2H_6 and C_2H_4 adsorption sites in Cr-BTC (a, c) and Cr-BTC(O_2) (b, d) obtained from DFT calculations (Cr, navy; C, gray; O, red; O_2^-, orange; H, white).

Optimal gas binding configurations were identified and are shown in Fig. 3(b, d). C_2H_6 exhibits a larger affinity than C_2H_4 toward the superoxo group, through stronger O…H interaction (the hydrogen bond distance: 0.30 nm *vs* 0.33 nm). The stronger C_2H_6 binding is also partly due to the molecular geometry of C_2H_6 (trigonal pyramidal shape, in contrast to the trigonal planar shape of C_2H_4), which enables a better van der Waals interaction with the surrounding ligand surfaces in this particular MOF structure. As a net result, the calculated static binding energies of C_2H_4 and C_2H_6 on the superoxo site are 21.0 and 28.7 $kJ \cdot mol^{-1}$, respectively. Apparently, the effect of the superoxo functionalization in the structure is two-fold: a notable C_2H_6 binding enhancement, and a significant C_2H_4 binding strength reduction. Consequently, the binding preference between the two gases are reversed. These results are fully consistent with our experimental observations, and well explain the adsorption mechanisms qualitatively.

4. Conclusions

In summary, we have realized a functionalized MOF for the challenging task of C_2H_6/C_2H_4 separation. The basic mechanism of this MOF for the specific recognition of C_2H_6 has been clearly demonstrated through theoretical calculations. With the introduction of superoxo groups, Cr-BTC(O_2) exhibits a higher binding affinity for C_2H_6 molecule, which realizes the efficient C_2H_6/C_2H_4 mixture separations under ambient conditions to directly produce high-purity C_2H_4. This work will provide a feasible strategy on the modification of OMSs within MOFs for stronger interactions with C_2H_6 than with C_2H_4, and prepare some useful porous materials for realization of the challenging C_2H_6/C_2H_4 separation.

Acknowledgments

We gratefully acknowledge the financial support from the National Natural Science Foundation of China (Nos. 21606163 and 21878205), Coal Bed Methane Joint Foundation of Shanxi (2016012006), Foundation of State Key Laboratory of Coal Conversion (J18-19-610), Welch Foundation (grant AX-1730), and the Distinguished Scientist Fellowship Program (DSFP) at KSU.

Supplementary Material

Supplementary data to this article can be found online at https://doi.org/10.1016/j.cjche.2019.09.005.

References

[1] P.Q. Liao, W.X. Zhang, J.P. Zhang, X.M. Chen, Efficient purification of ethene by an ethane-trapping metal-organic framework, *Nat. Commun.* 6 (2015) 8697.
[2] J.R. Li, R.J. Kuppler, H.C. Zhou, Selective gas adsorption and separation in metal-organic frameworks, *Chem. Soc. Rev.* 38 (5) (2009) 1477–1504.
[3] D.S. Sholl, R.P. Lively, Seven chemical separations to change the world, *Nature* 532 (7600) (2016) 435–437.
[4] P.J. Bereciartua, Á. Cantín, A. Corma, J.L. Jordá, M. Palomino, F. Rey, S. Valencia, E.W. Corcoran, P. Kortunov, P.I. Ravikovitch, A. Burton, C. Yoon, Y. Wang, C. Paur, J. Guzman, A.R. Bishop, G.L. Casty, Control of zeolite framework flexibility and pore topology for separation of ethane and ethylene, *Science* 358 (6366) (2017) 1068–1071.
[5] K. Adil, Y. Belmabkhout, R.S. Pillai, A. Cadiau, P.M. Bhatt, A.H. Assen, G. Maurin, M. Eddaoudi, Gas/vapour separation using ultra-microporous metal-organic frameworks: insights into the structure/separation relationship, *Chem. Soc. Rev.* 46 (11) (2017) 3402–3405.
[6] R.B. Lin, S.C. Xiang, H.B. Xing, W. Zhou, B.L. Chen, Exploration of porous metal-organic frameworks for gas separation and purification, *Coord. Chem. Rev.* 378 (2019) 87–103.
[7] C. Gu, N. Hosono, J.-J. Zheng, Y. Sato, S. Kusaka, S. Sakaki, S. Kitagawa, Design and control of gas diffusion process in a nanoporous soft crystal, *Science* 363 (6425) (2019) 387–391.
[8] H. Wang, X.L. Dong, V. Colombo, Q.N. Wang, Y.Y. Liu, W. Liu, X.L. Wang, X.Y. Huang, D.M. Proserpio, A. Sironi, Y. Han, J. Li, Tailor-made microporous metal-organic frameworks for the full separation of propane from propylene through selective size exclusion, *Adv. Mater.* 30 (49) (2018), 1805088.
[9] X. Zhao, Y. Wang, D.-S. Li, X. Bu, P. Feng, Metal-organic frameworks for separation, *Adv. Mater.* 30 (49) (2018), 1705189.
[10] L. Li, H. Wen, C. He, R.B. Lin, R. Krishna, H. Wu, W. Zhou, J. Li, B. Li, B. Chen, A metal-organic framework with suitable pore size and specific functional sites for the removal of trace propyne from propylene, *Angew. Chem. Int. Ed.* 57 (46) (2018) 15183–15188.
[11] P.Q. Liao, N.Y. Huang, W.X. Zhang, J.P. Zhang, X.M. Chen, Controlling guest conformation for efficient purification of butadiene, *Science* 356 (6343) (2017) 1193–1196.
[12] L. Li, R.B. Lin, R. Krishna, X. Wang, B. Li, H. Wu, Flexible-robust metal-organic framework for efficient removal of propyne from propylene, *J. Am. Chem. Soc.* 139 (23) (2017) 7733–7736.
[13] B. Li, X.L. Cui, D. O'Nolan, H.M. Wen, M.D. Jiang, R. Krishna, H. Wu, R.B. Lin, Y.S. Chen, D.Q. Yuan, H.B. Xing, W. Zhou, Q.L. Ren, G.D. Qian, M.J. Zaworotko, B.L. Chen, An ideal

molecular sieve for acetylene removal from ethylene with record selectivity and productivity, *Adv. Mater.* 29 (47) (2017), 1704210.
[14] X.L. Cui, K.J. Chen, H.B. Xing, Q.W. Yang, R. Krishna, Z.B. Bao, H. Wu, W. Zhou, X.L. Dong, Y. Han, B. Li, Q.L. Ren, M.J. Zaworotko, B.L. Chen, Pore chemistry and size control in hybrid porous materials for acetylene capture from ethylene, *Science* 353 (6295) (2016) 141–144.
[15] A. Cadiau, K. Adil, P.M. Bhatt, Y. Belmabkhout, M. Eddaoudi, A metal-organic framework-based splitter for separating propylene from propane, *Science* 353 (6295) (2016) 137–140.
[16] Z. Bao, G. Chang, H. Xing, R. Krishna, Q. Ren, B. Chen, Potential of microporous metal–organic frameworks for separation of hydrocarbon mixtures, *Energy Environ. Sci.* 9 (12) (2016) 3612–3641.
[17] M.L. Foo, R. Matsuda, Y. Hijikata, R. Krishna, H. Sato, S. Horike, A. Hori, J.G. Duan, Y. Sato, Y. Kubota, M. Takata, S. Kitagawa, An adsorbate discriminatory gate effect in a flexible porous coordination polymer for selective adsorption of CO_2 over C_2H_2, *J. Am. Chem. Soc.* 138 (9) (2016) 3022–3030.
[18] P. Nugent, Y. Belmabkhout, S.D. Burd, A.J. Cairns, R. Luebke, K. Forrest, T. Pham, S. Ma, B. Space, L. Wojtas, M. Eddaoudi, M.J. Zaworotko, Porous materials with optimal adsorption thermodynamics and kinetics for CO_2 separation, *Nature* 495 (7439) (2013) 80–84.
[19] K. Li, D.H. Olson, J. Seidel, T.J. Emge, H. Gong, H. Zeng, J. Li, Zeolitic imidazolate frameworks for kinetic separation of propane and propene, *J. Am. Chem. Soc.* 131 (30) (2009) 10368–10369.
[20] H. Furukawa, K.E. Cordova, M. O'Keeffe, O.M. Yaghi, The chemistry and applications of metal-organic frameworks, *Science* 341 (6149) (2013), 1230444.
[21] S. Kitagawa, R. Kitaura, S. Noro, Functional porous coordination polymers, *Angew. Chem. Int. Ed.* 43 (18) (2004) 2334–2375.
[22] H. Li, L. Li, R.B. Lin, W. Zhou, Z. Zhang, S. Xiang, B. Chen, Porous metal-organic frameworks for gas storage and separation: Status and challenges, *Energy Chem.* 1 (1) (2019)100006.
[23] P. Li, Q. Chen, T.C. Wang, N.A. Vermeulen, B.L. Mehdi, A. Dohnalkoya, N.D. Browning, D. Shen, R. Anderson, D.A. Gomez-Gualdron, F.M. Cetin, J. Jagiello, A.M. Asiri, J.F. Stoddart, O.K. Farha, Hierarchically engineered mesoporous metal-organic frameworks toward cell-free immobilized enzyme systems, *Chem* 4 (5) (2018) 1022–1034.
[24] C. Wang, D. Liu, W. Lin, Metal-organic frameworks as a tunable platform for designing functional molecular materials, *J. Am. Chem. Soc.* 135 (36) (2013) 13222–13234.
[25] B. Chen, S. Xiang, G. Qian, Metal-organic frameworks with functional pores for recognition of small molecules, *Acc. Chem. Res.* 43 (8) (2010) 1115–1124.
[26] B. Li, M. Chrzanowski, Y. Zhang, S. Ma, Applications of metal-organic frameworks featuring multi-functional sites, *Coord. Chem. Rev.* 307 (2016) 106–129.
[27] S. Yang, A.J. Ramirez-Cuesta, R. Newby, V. Garcia-Sakai, P. Manuel, S.K. Callear, S.I. Campbell, C.C. Tang, M. Schröder, Supramolecular binding and separation of hydrocarbons within a functionalized porous metal–organic framework, *Nat. Chem.* 7 (2) (2015) 121–129.
[28] Y. Bai, Y. Dou, L.-H. Xie, W. Rutledge, J.-R. Li, H.-C. Zhou, Zr-based metal-organic frameworks: design, synthesis, structure, and applications, *Chem. Soc. Rev.* 45 (8) (2016) 2327–2367.
[29] Q.L. Zhu, Q. Xu, Metal-organic framework composites, *Chem. Soc. Rev.* 43 (16) (2014) 5468–5512.
[30] Q.G. Zhai, X.H. Bu, C.Y. Mao, X. Zhao, L. Daemen, Y.Q. Cheng, A.J. Ramirez-Cuesta, P.Y. Feng, An ultra-tunable platform for molecular engineering of high-performance crystalline porous materials, *Nat. Commun.* 7 (2016), 13645.
[31] E.D. Bloch, W.L. Queen, R. Krishna, J.M. Zadrozny, C.M. Brown, J.R. Long, Hydrocarbon separations in a metal-organic framework with open iron(II) coordination sites, *Science* 335 (6076) (2012) 1606–1610.
[32] R.B. Lin, L. Li, H.L. Zhou, H. Wu, C.H. He, S. Li, R. Krishna, J. Li, W. Zhou, B. Chen, Molecular sieving of ethylene from ethane using a rigid metal–organic framework, *Nat. Mater.* 17 (12) (2018) 1128–1133.
[33] R.-B. Lin, H. Wu, L. Li, X.-L. Tang, Z. Li, J. Gao, H. Cui, W. Zhou, B. Chen, Boosting ethane/ethylene separation within Isoreticular Ultramicroporous metal-organic frameworks, *J. Am. Chem. Soc.* 140 (40) (2018) 12940–12946.
[34] O.T. Qazvini, R. Babarao, Z.L. Shi, Y.B. Zhang, S.G. Telfer, A robust ethane-trapping metal-organic framework with a high capacity for ethylene purification, *J. Am. Chem. Soc.* 141 (12) (2019) 5014–5020.
[35] C. Gücüyener, J. van den Bergh, J. Gascon, F. Kapteijn, Ethane/ethene separation turned on its head: selective ethane adsorption on the metal-organic framework ZIF-7 through a gate-opening mechanism, *J. Am. Chem. Soc.* 132 (50) (2010) 17704–17706.
[36] J. Pires, M.L. Pinto, V.K. Saini, Ethane selective IRMOF-8 and its significance in ethane-ethylene separation by adsorption, *ACS Appl. Mater. Interfaces* 6 (15) (2014) 12093–12099.
[37] Y. Chen, Z. Qiao, H. Wu, D. Lv, R. Shi, Q. Xia, J. Zhou, Z. Li, An ethane-trapping MOF PCN-250 for highly selective adsorption of ethane over ethylene, *Chem. Eng. Sci.* 175 (2018) 110–117.
[38] L. Li, R.-B. Lin, R. Krishna, H. Li, S. Xiang, H. Wu, J. Li, W. Zhou, B. Chen, Ethane/ethylene separation in a metal-organic framework with iron-peroxo sites, *Science* 362 (6413) (2018) 443–446.
[39] L.J. Murray, M. Dinca, J. Yano, S. Chavan, S. Bordiga, C.M. Brown, J.R. Long, Highly-Selective and reversible O_2 binding in Cr_3(1,3,5-benzenetricarboxylate)$_2$, *J. Am. Chem. Soc.* 132 (23) (2010) 7856–7857.